THE JOURNAL OF BIOLOGICAL CHEMISTRY VOL. 286, NO. 20, pp. 18149–18160, May 20, 2011

Effect of Kallikrein 4 Loss on Enamel Mineralization

*COMPARISON WITH MICE LACKING MATRIX METALLOPROTEINASE 20**

Received for publication, October 13, 2010, and in revised form, March 3, 2011 Published, JBC Papers in Press, March 23, 2011, DOI 10.1074/jbc.M110.194258

Charles E. Smith[‡§1], Amelia S. Richardson[§], Yuanyuan Hu[§], John D. Bartlett[¶], Jan C-C. Hu[§], and James P. Simmer[§]

From the [‡]Facility for Electron Microscopy Research, Department of Anatomy and Cell Biology and Faculty of Dentistry, McGill University, Montreal, Quebec H3A 2B2, Canada, the [§]Department of Biologic and Materials Sciences, University of Michigan School of Dentistry, Ann Arbor, Michigan 48108, and the [¶]Department of Cytokine Biology, Forsyth Institute and Department of Developmental Biology, Harvard School of Dental Medicine, Boston, Massachusetts 02142

Enamel formation depends on a triad of tissue-specific matrix proteins (amelogenin, ameloblastin, and enamelin) to help initiate and stabilize progressively elongating, thin mineral ribbons of hydroxyapatite formed during an appositional growth phase. Subsequently, these proteins are eradicated to facilitate lateral expansion of the hydroxyapatite crystallites. The purpose of this study was to investigate changes in enamel mineralization occurring in mice unable to produce kallikrein 4 (Klk4), a proteinase associated with terminal extracellular degradation of matrix proteins during the maturation stage. Mice lacking functional matrix metalloproteinase 20 (Mmp20), a proteinase associated with early cleavage of matrix proteins during the secretory stage, were also analyzed as a frame of reference. The results indicated that mice lacking Klk4 produce enamel that is normal in thickness and overall organization in terms of layers and rod/inter-rod structure, but there is a developmental defect in enamel rods where they first form near the dentinoenamel junction. Mineralization is normal up to early maturation after which the enamel both retains and gains additional proteins and is unable to mature beyond 85% mineral by weight. The outmost enamel is hard, but inner regions are soft and contain much more protein than normal. The rate of mineral acquisition overall is lower by 25%. Mice lacking functional Mmp20 produce enamel that is thin and structurally abnormal. Relatively high amounts of protein remain throughout maturation, but the enamel is able to change from 67 to 75% mineral by weight during maturation. These findings reaffirm the importance of secreted proteinases to enamel mineral acquisition.

The mechanisms by which ameloblasts induce, lengthen, and control changes in the size of hydroxyapatite crystallites they organize into characteristic rod and inter-rod patterns in mammalian enamel have remained largely undefined for the past 6 decades (1, 2). What has improved is the level of understanding about the various proteins these cells secrete to form and modify the organic matrix of developing enamel and the genes that encode each of these components (3–5). Among many surprises that have arisen is the discovery that ameloblasts secrete two protein altering enzymes as follows: one in tandem with matrix proteins as the enamel layer is being created and another later in time to help promote maturation (expansion) of incompletely developed enamel crystallites (6). If either one of these two proteinases is functionally defective or missing, the enamel produced is grossly defective and/or inferior in quality (7–10).

The two secreted proteinases that have been identified as essential participants in amelogenesis are matrix metalloproteinase 20 (Mmp20) (8) and kallikrein 4 (Klk4) (10). Mmp20 is expressed throughout the secretory stage (11). Klk4, however, is expressed during the maturation stage, including the short transitional phase when ameloblasts undergo reorganization from functional activities associated with appositional growth of the enamel layer to those associated with ion transport and mineral deposition (9, 11–13). Both proteinases are secreted in a latent proenzyme form, but how each is activated remains poorly defined at present (6, 14). Mmp20 is responsible for making several initial, specific, and rapid cleavages on newly secreted high abundance amelogenins enamel matrix proteins as well as on each of the two relatively low abundance non-amelogenin enamel matrix proteins, ameloblastin and enamelin (15–17). Fragments from these cleavages in some species take on specific distribution patterns within the developing enamel layer both in relation to rod and inter-rod areas and to depth in a direction from the dentinoenamel junction (DEJ)[2] to the forming outer surface (18). Klk4 appears to function primarily as an intermediary to further degrade fragments created from amelogenin, ameloblastin, and enamelin processing by Mmp20, thereby facilitating their removal from the enamel layer presumably assisted by resorptive activity of modulating ameloblasts as part of the maturation process (6). How Klk4 penetrates the surface basal lamina and partially mineralized enamel at the surface and moves within the depth of the hardening enamel layer as it matures is currently undefined. The life span and long term fate of both Mmp20 and Klk4 within the enamel layer are also poorly understood.

It has been known for many years from an engineered mouse model that Mmp20 loss-of-function has disastrous consequences to both the formation and the maturation of enamel (7). The incisors and molars of *Mmp20* null mice are covered by a thin layer of low quality enamel that chips easily away from the dentin, contains little or no decussating rod and inter-rod sub-

* This work was supported, in whole or in part, by National Institutes of Health Grants DE019775 and DE016276 from NIDCR.

[1] To whom correspondence should be addressed: Dept. of Anatomy and Cell Biology, McGill University, 3640 University St., Montreal, Quebec H3A 2B2, Canada. Tel.: 514-398-4520; Fax: 514-398-5047; E-mail: charles.smith@mcgill.ca.

[2] The abbreviations used are: DEJ, dentinoenamel junction; SEM, scanning electron microscopy.

structure, and is much softer than normal (7, 19). This contrasts with a recently described mouse model for Klk4 loss-of-function where the teeth of null mice are covered by enamel that is normal in thickness and has a characteristic layered organization with typical rod and inter-rod substructure (9). Maturation and hardening of the enamel in these animals are delayed, however, and there is a defect in mineralization internally near the DEJ such that the enamel on erupted crowns fractures off at sites where opposing teeth come into physical contact with one another. This causes molars to undergo abnormal wear, and the incisors to show chipped incisal ends (9).

The purpose of this study was to obtain a more detailed understanding of the timing and changes occurring within the organic and mineral phases of developing enamel on the teeth of mice unable to produce either Klk4 or Mmp20. This study takes advantage of the newly engineered *Klk4* knock-out/*lacZ* knock-in mouse model (9) and the well defined *Mmp20* loss-of-function mouse model described originally in 2002 (7). Although some basic quantitative information about changes in the mineral content in enamel by stages was published for Mmp20 (19), this investigation uses a newly bred set of mice to look at individual step-by-step changes across the entire length of continuously erupting incisors as well as bulk changes in molars. As documented herein, mild heterozygous effects on protein and mineral content are detected in maturing enamel with both mouse models. Mice that are null for Klk4 show two times below normal mineral-to-protein ratios, whereas those that are null for Mmp20 show four times lower ratios at a time in development when the enamel in wild-type mice hardens to the point where it cannot be cut with a scalpel blade. In both cases, this is caused in part by grossly elevated levels of protein present at a time when inter-crystalline spaces in healthy wild-type mice are normally filled primarily with tissue (enamel) fluid (12).

EXPERIMENTAL PROCEDURES

Animals—All procedures involving animals were reviewed and approved by the Institutional Animal Care and Use Committees of the University of Michigan and the Forsyth Institute. Klk4 loss-of-function ($Klk4^{-/-}$; $Klk4^{+/-}$) and wild-type ($Klk4^{+/+}$) jaw samples were obtained from a breeding colony maintained in a C57BL/6 background and housed at the University of Michigan. The *Klk4* coding region in these mice was deleted in its entirety and replaced with a bacterial *lacZ* nuclear reporter gene (9). Animals of all *Klk4* genotypes were fed a soft diet (DietGel^{TM} R/L; ClearH_2O, Portland, ME), which yielded better survival of null mice after weaning than regular hard rodent chow (9). Mmp20 loss-of-function ($Mmp20^{-/-}$; $Mmp20^{+/-}$) and wild-type ($Mmp20^{+/+}$) jaw samples were obtained from a breeding colony also maintained in a C57BL/6 background and housed at the Forsyth Institute. The *Mmp20* gene in these mice was altered such that most of intron 4 as well as the zinc-binding site essential for the catalytic activity of the proteinase in exon 5 were deleted (7). Animals of all *Mmp20* genotypes were fed a standard hard rodent chow diet (LabDiet Rodent Diet 5053, PharmaServ, Framingham, MA). Genotyping in all cases was carried out by PCR on genomic DNA obtained from tail biopsies (7, 9).

Sample Preparations and Processing—Hemi-maxillae and hemi-mandibles from terminally narcosed 7-week-old male and female mice were removed and rapidly cleaned of skin, hair, and adhering muscular tissues. The hemi-jaws were flash-frozen in prechilled containers surrounded with dry ice. The samples were stored in a −80 °C freezer and then shipped on dry ice from Ann Arbor (*Klk4* group) and Boston (*Mmp20* group) to Montreal. All hemi-jaws were freeze-dried for 48 h at −55 °C (Labconco, Kansas City, MO) and stored thereafter at 4 °C in screw top containers with Drierite (Fisher). Procedures for processing whole molars and small samples of bone, dentin, and sequential 1-mm-long strips of enamel organ cells and developing enamel from maxillary and mandibular incisors by free hand dissection for mineral analyses by heating and micro weighing have been described in detail in previous reports (20, 21). Briefly, individual samples were first weighed on an SC2 microbalance (Sartorius, Göttingen, Germany) and then placed in an Isotemp muffle furnace (Fisher) where they were heated at 575 °C for 18 h. Each sample was cooled and reweighed. This procedure vaporizes (ashes) organic material and any bound water, leaving behind the mineral residue contained within the sample (20). These directly measured "before" and "after" ashing weights were used to calculate other parameters, including (*a*) weight of volatiles per sample (before ashing weight − after ashing weight), (*b*) percent mineral by weight (after ashing weight/before ashing weight × 100), and (*c*) mineral-to-volatiles ratio (after ashing weight/weight of volatiles per sample). In addition, data from sequential strip dissections on incisors were used to estimate the total mineral gain per mm (mineral acquisition rate) by subtracting the mineral weight of a previous strip from the mineral weight of the current strip, sequentially across all 1-mm-long strips in a series.

Data Collection and Statistical Analyses—Weight data for enamel strips, and for pieces of dentin and bone, were collected from a minimum of 12 maxillary and 12 mandibular samples per genotype ($12 \times 2 \times 6 = 144$ hemi-jaws overall). Weight data for enamel organ cell strips were obtained from a separate set of maxillary and mandibular incisors from four wild-type (+/+) and four heterozygous (+/−) mice and from six null (−/−) mice in the *Klk4* and *Mmp20* groups ($2 \times (4 + 4 + 6) \times 2 = 56$ hemi-jaws). Weight data for whole maxillary and mandibular molars were obtained from four mice per genotype ($2 \times 4 \times 6 = 48$ hemi-jaws $\times$ 3 molars per hemi-jaw $= 144$ molars sampled overall). Means and confidence intervals for weight data and univariate factorial analysis of variance were obtained using version 9 of Statistica for Windows (StatSoft, Tulsa, OK). For these analyses, strip 1 on maxillary incisors and strips 1 + 2 on mandibular incisors were defined as secretory stage; strips 2 + 3, 4 + 5, and 6 + 7 on maxillary incisors and strips 3 + 4, 5 + 6, and 7 + 8 + 9 on mandibular incisors were classified as early, mid, and late maturation stage; and strips 7 + 8 on maxillary incisors and strips 9 + 10 + 11 + 12 on mandibular incisors were designated as part of the exposed erupted portion of the incisor.

Scanning Electron Microscopy (SEM)—At least six freeze-dried hemi-mandibles from 7-week-old mice of each genotype in the *Klk4* and *Mmp20* groups were prepared for scanning electron microscopy of the incisors and molars. For incisor

TABLE 1
Percent mineral by weight for dentin and bone
$n = 12$ incisors or hemi-jaws per genotype.

Genotype	Dentin, incisor	Bone, maxilla	Bone, mandible
$Klk4^{+/+}$	73.9 ± 0.7	68.8 ± 1.3	71.2 ± 1.0
$Klk4^{+/-}$	74.4 ± 0.8	69.7 ± 1.3	72.2 ± 0.7
$Klk4^{-/-}$	74.9 ± 0.7	68.6 ± 0.7	72.0 ± 0.9
$Mmp20^{+/+}$	73.1 ± 1.8	68.4 ± 2.2	70.4 ± 2.4
$Mmp20^{+/-}$	71.6 ± 0.5	68.3 ± 2.2	71.0 ± 2.5
$Mmp20^{-/-}$	73.6 ± 0.9	69.0 ± 2.2	71.4 ± 2.5

imaging, the bony caps covering the developing teeth were removed, and the enamel organ cells were gently elevated and/or brushed away from the developing enamel surfaces on the incisors and discarded. The exposed enamel surfaces were delicately wiped with dry Kimwipes, and the incisors were examined at ×50 magnification without any further processing in a Hitachi S-3000N variable pressure scanning electron microscope using the backscatter mode at 25 kV and 20 pascal pressure. For molars, the gingiva and associated connective tissues surrounding the roots of the molar crowns were carefully dissected away, and the crowns were cleaned of any associated food particles or blood using a scalpel blade followed by gentle wiping with a gauze pad moistened with 2% hypochlorite solution and rinsing with distilled water. The molars were air-dried and then imaged without further processing in backscatter mode at ×40 magnification using 15–30 kV and 20 pascal pressure. In other experiments, freeze-dried hemi-mandibles from 9-week-old wild-type ($Klk4^{+/+}$) and $Klk4^{-/-}$ and $Mmp20^{-/-}$ (null) mice were cleaned of muscle and soft tissues and embedded directly in Castolite Formula AC clear plastic resin (Castolite Co., Woodstock, IL). After polymerization, the incisors were cut transversely (cross-section) with a model 650 low speed diamond wheel saw (South Bay Technology Inc., San Clemente, CA) at the level of the crest of the alveolar bone close to where the incisor erupts into the mouth. The sectioned hemi-mandibles were then re-embedded in Castolite using 25-mm SteriForm molds (Struers Inc., Westlake, OH). The transversely sectioned faces of the mandibular incisors were polished sequentially with a Syntron Polisher on 120, 180, and 400 waterproof silicon carbide papers followed by polishing on glass with 800 silicon powder and then overnight with 1 μm diamond powder (Mager Scientific Inc., Dexter, MI). The polished surfaces were examined at ×50 magnification in a Cameca SX-100 electron microprobe analyzer using the backscatter mode at 15 kV and a calibration wedge to ensure that the range of intensities in each image recorded spanned a similar range of gray level intensities. Four-level color mapping was done using ImageJ (/rsb.info.nih.gov) on Tiff images that were normalized to have the same mean gray level intensities for mineralized dentin (dentin and bone show no significant changes in mineral content by genotype; see Table 1).

RESULTS

Effects of Loss of Function of Klk4 and Mmp20 on Enamel Organ Cells—Sequential strip dissections of 1-mm-long pieces of freeze-dried enamel organ cells from the labial surface of mouse incisors in each of six genotypes ($Klk4^{+/+}$, $Klk4^{+/-}$, $Klk4^{-/-}$, $Mmp20^{+/+}$, $Mmp20^{+/-}$, and $Mmp20^{-/-}$) indicated

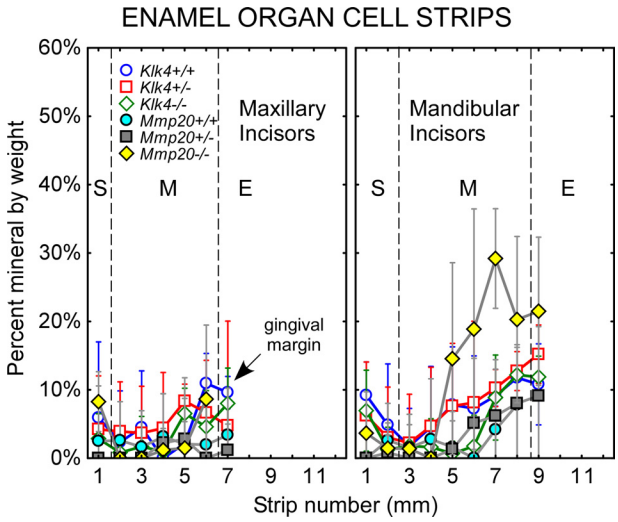

FIGURE 1. **Mineral content in enamel organ cells from maxillary and mandibular incisors of wild-type ($Klk4^{+/+}$, $Mmp20^{+/+}$), heterozygous ($Klk4^{+/-}$, $Mmp20^{+/-}$), and null ($Klk4^{-/-}$, $Mmp20^{-/-}$) mice.** Mean plots ± 95% confidence intervals of the percent mineral by weight in 1-mm-long freeze-dried cell strips dissected across the portion of the incisor embedded in bone (*S*+*M*). Most cell samples are associated with little mineral except in the case of mandibular incisors from $Mmp20^{-/-}$ mice (*yellow diamonds*). The large deviations indicate there is considerable tooth-to-tooth variation in mineral-promoting responses by enamel organ cells to loss-of-function of Mmp20 across the mid- to late stages of maturation. *S,* secretory stage; *M,* maturation stage; *E,* erupted portion.

little mineral (0–10% by weight) associated with the cell layers other than an occasional flake of bone or enamel contaminating the sample (random noise) (Fig. 1). One exception was enamel organ cell samples taken from the mandibular incisors of $Mmp20^{-/-}$ mice, which showed above average and increasing amounts of mineral at sites associated with mid- to late maturation phases of amelogenesis (Fig. 1, *strips 5–7*). There was considerable variation, however, between mandibular incisors in the amounts of mineral present within the cell layers with some teeth showing near normal amounts (0–10% by weight) and others having very high levels of mineral (as high as 40% by weight) (Fig. 1, deviations indicated by wide deviation bars on *yellow diamonds*). The quantity of mineral associated with enamel organ cell layers in $Mmp20^{-/-}$ mice was considerably less than amounts previously detected for mice lacking either enamelin or ameloblastin (21).

Scanning Electron Microscopy of Developing Enamel Surfaces on Incisors—The enamel surfaces on freeze-dried incisors from wild-type mice appeared by backscatter electron imaging to be relatively smooth from apical (secretory) to incisal (erupted) ends (Fig. 2, *A*, $Klk4^{+/+}$, and *B*, $Mmp20^{+/+}$). The secretory zone at the apical end typically appeared dark due to its high content of organic material, whereas more incisally located maturing and mature areas of the enamel had a white appearance and in some cases slightly undulating appearance especially along the erupted portion at the incisal end. The enamel surfaces of incisors from heterozygous $Klk4^{+/-}$ and $Mmp20^{+/-}$ mice appeared overall similar to wild-type controls (Fig. 2, *A* and *B*). For both genotypes, there was, however, the suggestion of more surface irregularities and crazing of the enamel surfaces in the transitional areas between secretory and early maturation zones (Fig. 2, *A* and *B, middle rows, panels to*

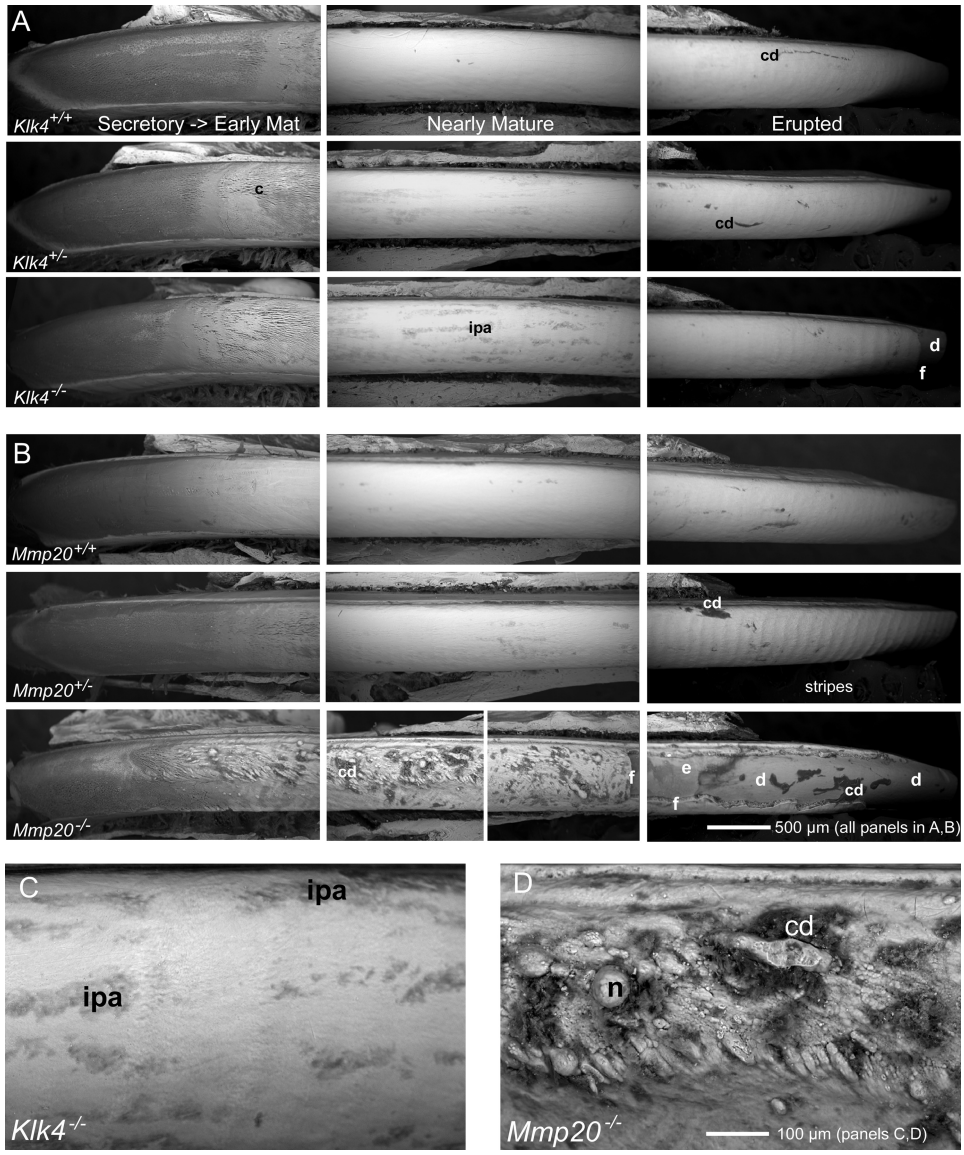

FIGURE 2. **Scanning electron microscopy in backscatter mode at low (*A* and *B*) and high (*C* and *D*) magnifications showing developing enamel surfaces along the labial side of incisors in the apical (secretory to early maturation), middle (nearly mature), and incisal (erupted) ends of teeth from wild-type (*A, Klk4*$^{+/+}$*; B, Mmp20*$^{+/+}$), heterozygous (*A, Klk4*$^{+/-}$*; B, Mmp20*$^{+/-}$), and null (*A, Klk4*$^{-/-}$*; B, Mmp20*$^{-/-}$) mice.** In this technique, *whiter areas* contain more mineral than *darker areas*. The enamel surfaces of incisors in wild-type (+/+) mice appear relatively smooth and mostly devoid of cell debris (*cd*) across their length (*A* and *B*; *top rows, all panels*). Enamel surfaces of incisors in *Klk4*$^{+/-}$ (*A*) and *Mmp20*$^{+/-}$ (*B*) mice appear similar to wild-type mice except in early maturation where cracks (*c*) from freeze drying are sometimes more prominent (*A* and *B*; *top* and *middle rows, left panels*). The incisors of *Mmp20*$^{+/-}$ mice also consistently show regularly spaced surface undulations (*stripes*) in enamel running perpendicular to the long axis of the tooth across the erupted portion of the tooth (*B, middle row, right panel*). The enamel surfaces on incisors from *Klk4*$^{-/-}$ mice are relatively smooth, although irregular pitted areas (*ipa*) are seen across regions where the enamel becomes nearly mature (*A, bottom row, middle panel,* and *C*). The enamel along the erupted portions of these incisors often shows faint stripes and is consistently fractured (*f*) near the incisal tips exposing the underlying dentin (*d*) (*A, bottom row, right panel*). The enamel surfaces of incisors in *Mmp20*$^{-/-}$ mice are thin, rough, and obviously malformed (*B, bottom row*). Nodules (*n*) and other elongated calcified masses and associated cells debris (*cd*) project from the surface starting initially at the central labial aspect of the incisor in early maturation (*B, bottom row, left panel,* and *D*) and later across the whole labial surface of the tooth (*B, bottom row, middle panel*). The poorly formed mature enamel (*e*) is frail and easily fractures off (*f*) the erupted portions of these incisors exposing underlying dentin (*d*) (*B, bottom row, right panel*).

left). This transitional area in *Mmp20*$^{+/-}$ mice also consistently appeared somewhat darker compared with *Klk4*$^{+/-}$ mice and wild-type controls (Fig. 2, *A* and *B*). In addition, the erupted portions of both maxillary and mandibular incisors in *Mmp20*$^{+/-}$ mice universally showed a highly undulated surface in the form of regularly spaced and repeating stripes (22) spaced at about 80-μm intervals (Fig. 2*B, middle row, panel to right*). Surface striping was not prominent, although faintly evident, at the enamel surface across the erupted portions of incisors in *Klk4*$^{+/-}$ mice (Fig. 2*A*, *middle row, panel to right*). The enamel surfaces of incisors in *Klk4*$^{-/-}$ mice appeared somewhat more irregular and rough in texture compared with *Klk4*$^{+/-}$ and *Klk4*$^{+/+}$ mice, and they contained small, superficial focal areas irregularly distributed across the region of the tooth where the enamel matures that appeared organically rich (darker) (Fig. 2, *A, bottom row, middle panel,* and *C*). The enamel surfaces on the erupted portions of incisors in *Klk4*$^{-/-}$ mice also seemed slightly more undulated than in *Klk4*$^{+/-}$ mice, and the enamel near the incisal tips was consistently fractured away and/or noticeably worn down on all incisors (Fig. 2*A, bottom row, right*

panel). The enamel covering the incisors of *Mmp20*$^{-/-}$ mice was visually thinner than normal and was abnormal in appearance (Fig. 2*B, bottom row*, *all panels left* to *right*). These incisors showed nodular and rod-like masses of calcified material intermixed with cell debris distributed primarily along the central-labial aspect of the tooth in secretory and early maturation regions and at various sites across the whole labial side of the tooth in older (more incisal) regions where the enamel normally matures (Fig. 2, *B*, *bottom row, middle* and *right panels,* and *D*). The enamel covering the labial aspect of the erupted portion of the incisor was usually missing and fractured off the dentin at all sites except near the mesial and lateral cementoenamel junctions (Fig. 2*B*, *bottom row, right panel*).

Scanning Electron Microscopy of Incisor Enamel in Transverse Sections—Transverse ground sections of mandibular incisors at a site close to where these teeth erupt into the oral cavity as examined by backscatter mode indicated that mineral from wild-type mice was distributed fairly evenly throughout the depth of the enamel layer (Fig. 3*A*; thickness about 118 μm). There was, however, a trend for slightly increasing amounts of mineral to be present per unit area within the enamel layer progressing from the DEJ toward the outer enamel surface (Fig. 3, *A*, *top panels*, *numbers* in column to *right*, and *B*, *top panel*, *red versus blue colors*), which in part seemed to relate to the well defined "enamel spaces" normally present in rodent incisor enamel at the boundary between the initial and inner enamel layers (23–25), and to other microspaces present in inter-rod areas between enamel rods in this unfixed and freeze-dried material (Fig. 3*C*, *left panel*). Enamel in *Klk4*$^{-/-}$ (null) mice was similar in thickness (~117 μm) and overall structural organization as wild-type enamel in terms of laminated rod and inter-rod patterns and their grouping into inner and outer layers (Fig. 3*A, middle panel* compared with *top panel*). There was also the same trend as in wild-type mice for apparent increasing amounts of mineral measured per unit area from deeper to more superficial regions of the enamel layer (Fig. 3*A*, *middle panel,* compared with *top panel*, *numbers* in columns to *right*; Fig. 3*B*, *middle* and *top panels*, *red versus blue colors*), although the differential in the case of enamel from *Klk4*$^{-/-}$ mice was much greater than in the case of wild-type enamel (Fig. 3*A*, *middle* and *top panels*, 179/155 = 1.15 *versus* 194/190 = 1.02). The amount of microspaces both laterally and vertically between enamel rods in *Klk4*$^{-/-}$ mice appeared greater than in wild-type mice (Fig. 3, *B*, *middle* and *top panels*, *red versus blue colors,* and *C, middle versus left panels*). This in part caused enamel in *Klk4*$^{-/-}$ mice to appear to contain on average about 15% less mineral overall compared with wild-type enamel (Fig. 3, *A* and *B*). The enamel in *Klk4*$^{-/-}$ mice also appeared to have some developmental alterations near the DEJ such that the initial enamel layer applied to the dentin surface seemed to contain more mineral than the adjacent basal parts of enamel rods, which themselves looked poorly organized compared with sites farther away from the dentin (Fig. 3*C*, *middle panel* compared with *left panel*).

Enamel in *Mmp20*$^{-/-}$ (null) mice was thin (~40 μm) and poorly organized (Fig, 3*A, bottom panel* compared with *top panel*). It appeared to be arranged in three layers with the third outmost layer containing irregularly shaped nodular masses projecting away from the surface (Fig. 3, *A*, *bottom panel,* and *C, right panel*). The innermost layer abutting dentin was composed mostly of poorly mineralized, disorganized material and some spaces through which ran more highly mineralized short rod-like structures arrayed in a direction that was predominantly perpendicular to the DEJ (Fig. 3, *A*, *bottom panel,* and *C, right panel*, *dark versus light areas*; Fig. 3*B*, *bottom panel*, *blue, white,* and *red areas*). The middle layer appeared compact and relatively homogeneous by backscatter electron imaging (Fig. 3, *A*, *bottom panel,* and *C, right panel*) but in fact was composed of narrow and more heavily mineralized areas alternating with wider and less mineralized areas in a vertically banded arrangement (Fig. 3*B*, *bottom panel, blue versus red areas*). There was also a thin and more heavily mineralized line of material at the boundary between the middle and outermost layer (Fig. 3*B*, *bottom panel, red*). The outermost layer consisted of large tightly packed and more heavily mineralized areas alternating with large less mineralized areas that often had spaces at their core (Fig. 3, *A*, *bottom panel,* and *C, right panel, dark versus light areas*; Fig. 3*B*, *bottom panel, blue, white,* and *red areas*). The nodules projecting from this layer were composed mostly of less mineralized areas interspersed with irregularly shaped bands of more heavily mineralized material (Fig. 3*B*, *bottom panel, blue versus red areas*). There was the same trend as in wild-type and *Klk4*$^{-/-}$ mice for apparent increasing amounts of mineral measured per unit area from deeper to more superficial regions of the enamel layer (Fig. 3*A*, *bottom panel* compared with other panels, *numbers* in columns to *right*). The differential in average mineral content across the thickness of the enamel layer in the case of *Mmp20*$^{-/-}$ mice was large compared with wild-type and *Klk4*$^{-/-}$ mice (Fig. 3*A*, *bottom panel*, 180/133 = 1.35 *versus* 1.02 and 1.15). Interestingly, the average mineral content of enamel in the middle and outer layers of *Mmp20*$^{-/-}$ mice was very similar to the average mineral content in the same relative locations in *Klk4*$^{-/-}$ mice (Fig. 3*A*, *bottom* and *middle panels*). It was in the innermost layer closest to dentin that showed the greatest differences in mineral content between genotypes (Fig. 3*A*).

Mineral Content in Developing Enamel of Klk4 and Mmp20 Wild-type, Heterozygous, and Homozygous Null Mice—As found in previous studies (20, 21), both the starting dry weights (data not shown) and after ashing mineral weights of enamel strips removed from maxillary incisors of wild-type mice (*Klk4*$^{+/+}$, *Mmp20*$^{+/+}$) increased rapidly and progressively over 3–4 mm in the apical region of the tooth (Fig. 4, *A* and *D*). The same result was obtained for mandibular incisors except that strips could be removed over 5 mm of tooth length before the enamel was too hard to cut with a scalpel blade. The mean dry weight and mineral weight of strips from mandibular incisors was also 1.5–2-fold higher than in maxillary incisors (Fig. 4, *A* and *D*). The mean dry weight and mineral weight of enamel strips removed from maxillary incisors of heterozygous *Klk4*$^{+/-}$ and *Mmp20*$^{+/-}$ mice were very similar to wild-type mice (Fig. 4, *A* and *D*). However, it was possible to remove consistently one additional strip from the mandibular incisors of *Klk4*$^{+/-}$ mice (Fig. 4*A*, 6 mm). Enamel strips could be removed along the entire length of maxillary and mandibular incisors of homozygous *Klk4*$^{-/-}$ and *Mmp20*$^{-/-}$ mice (Fig. 4,

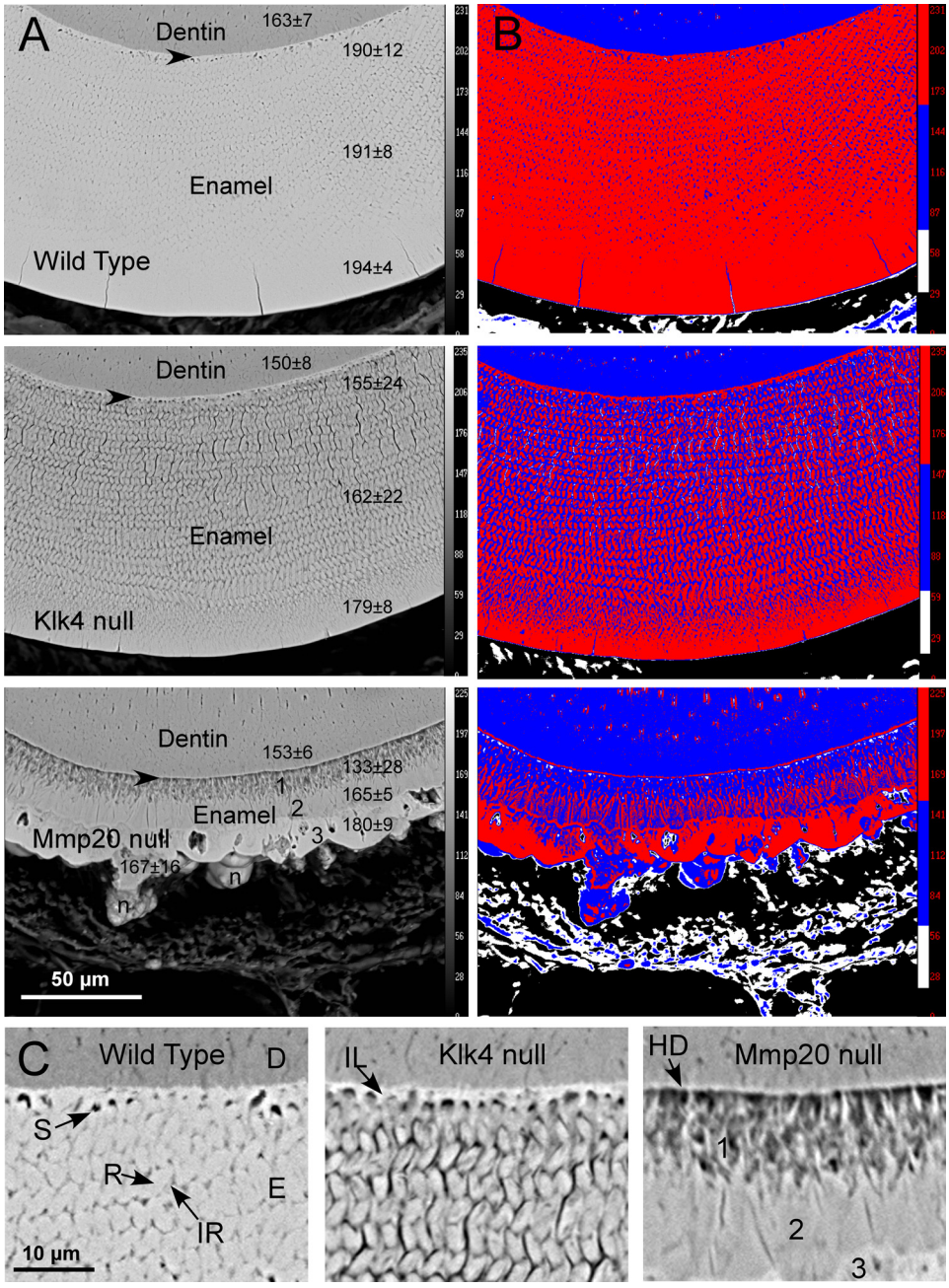

FIGURE 3. **Scanning electron microscopy in backscatter mode at low (*A* and *B*) and higher (*C*) magnifications of a portion of dentin and the entire enamel layer as seen in transverse ground sections of incisors from wild-type and *Klk4*$^{-/-}$ and *Mmp20*$^{-/-}$ mice cut at a level close to where the teeth erupt.** The images in *B* are pseudo colored maps of the same four gray level intensities for corresponding images in *A* (*red*, highest or most mineral). *Arrowheads* in *A* indicate approximate locations near the DEJ for images shown in *C*. The *numbers* in a column to the *right* of each image in *A* represent the mean gray level intensity ± S.D. counted within a 10 × 10 μm grid over dentin (*top numbers*) and the inner, middle, and outer regions of the enamel layer. In the *bottom panel* of *A*, the *numbers 1–3* indicate the tri-layered organization of enamel in *Mmp20*$^{-/-}$ mice; *n*, nodule of calcified material projecting from outer surface. *C, D* is dentin; *E* is enamel; *S* is normal developmental enamel spaces; *R* is enamel rod; *IR* is inter-rod enamel; *IL* is initial layer of enamel; *HD* is hypermineralized dentin. In wild-type and both *Klk4*$^{-/-}$ and *Mmp20*$^{-/-}$ mice, the outermost part of the enamel layer always appears more mineralized than the innermost part closest to dentin (*B, red versus blue colors*). Weaknesses in enamel observed in *Klk4*$^{-/-}$ and *Mmp20*$^{-/-}$ mice appear to be due in part to structural defects present near the DEJ (*C*) and to a less uniform distribution of mineral especially within inter-rod areas of the enamel (*B, blue* color compared with *red*).

A and *D*). The strips in *Klk4*$^{-/-}$ mice were very difficult to dissect because the outermost regions of the enamel on these teeth were hard enough to damage the scalpel blade from about mid-maturation all the way to the tip of the incisor (Fig. 4*A*, 4–5 to 8 or 12 mm). In these areas, the enamel was softer inside than at the surface, which provided a fracture plane by which strips could be lifted from the dentin and processed. The weight of mineral in these strips appeared to decrease progressively in a direction toward the incisal tips (Fig. 4*A*, 4–5 to 8 or 12 mm). Enamel strips in *Mmp20*$^{-/-}$ mice in contrast were thin and fragile and easy to remove across the entire length of the incisors (Fig. 4*D*, *yellow diamonds*). They contained only about one-third as much total mineral as wild-type controls (Fig. 4*D*). These strips also showed a similar although less pronounced trend to contain less mineral in a direction toward the erupted portion of the tooth (Fig. 4*D*).

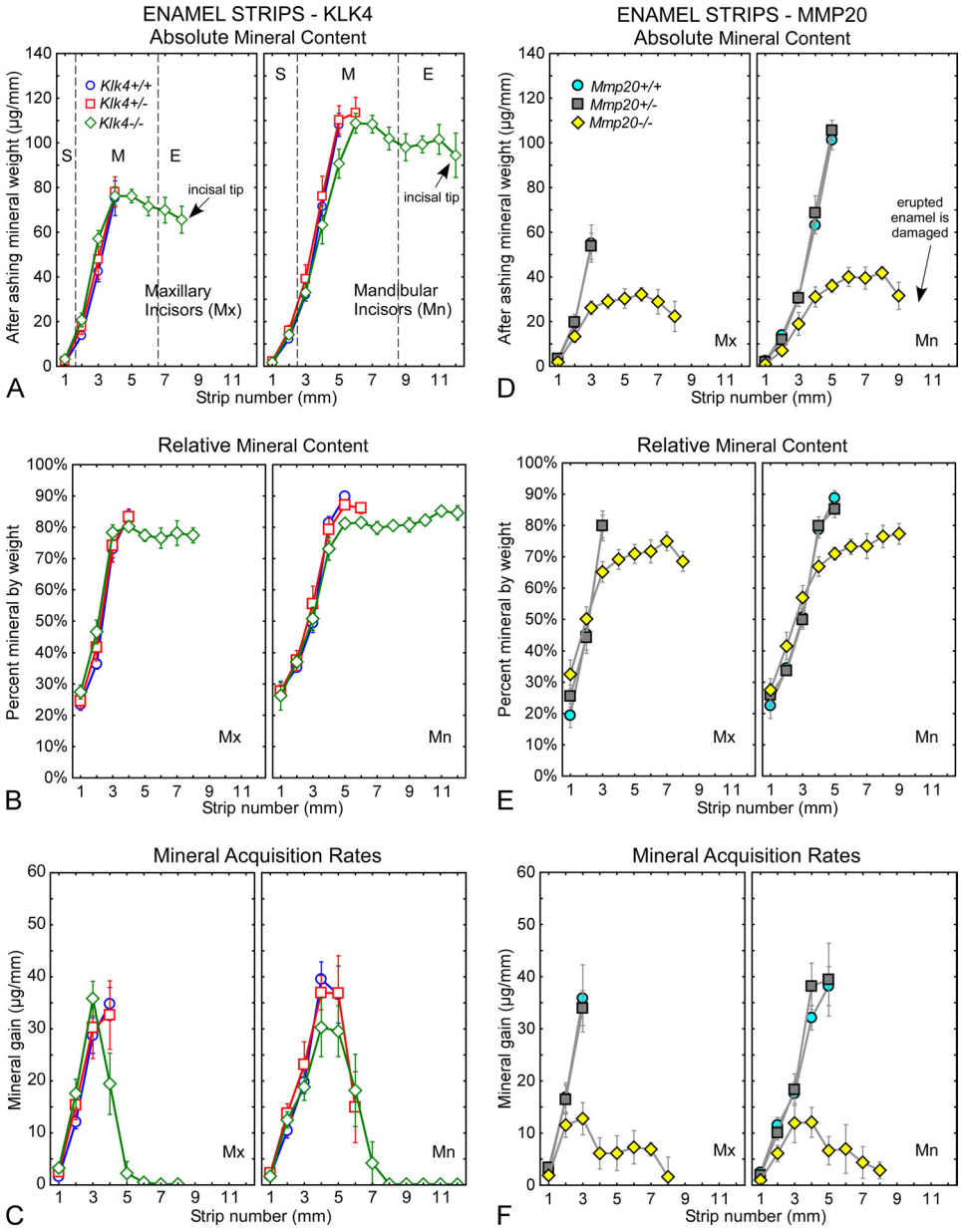

FIGURE 4. **Mineral content in enamel.** Absolute (*A* and *D*) and relative (*B* and *E*) mineral content and mineral acquisition rates (*C* and *F*) for developing enamel on incisors from wild-type (*A–C, Klk4*$^{+/+}$; *D–F, Mmp20*$^{+/+}$), heterozygous (*A–C, Klk4*$^{+/-}$; *D–F, Mmp20*$^{+/-}$), and null (*A–C, Klk4*$^{-/-}$; *D–F, Mmp20*$^{-/-}$) mice. Each *graph* represents mean ± 95% confidence intervals and shows after ashing weight (*A* and *D*), percent mineral by weight (*B* and *E*), and mineral gain per mm (*C* and *F*) for 1-mm-long enamel strips microdissected from maxillary (*left graph* each panel, *Mx*) and mandibular (*right graph* each panel, *Mn*) incisors. Stages of amelogenesis are illustrated by the *dashed lines* in *A* (*S*, secretory stage; *M*, maturation stage; *E*, erupted portion). Enamel in *Klk4*$^{-/-}$ mice is mildly hypomineralized across the maturation stage (*A–C*), whereas enamel in *Mmp20*$^{-/-}$ mice is both hypoplastic and hypomineralized (*D–F*). At its peak in early to mid-maturation (strip 4 on maxillary and strip 4–5 on mandibular incisors), *Klk4*$^{-/-}$ mice acquire mineral about 25% slower and *Mmp20*$^{-/-}$ mice about 70% slower than wild-type or heterozygous mice.

In relative terms, the enamel strips from maxillary and mandibular incisors of wild-type (*Klk4*$^{+/+}$, *Mmp20*$^{+/+}$) and heterozygous (*Klk4*$^{+/-}$, *Mmp20*$^{+/-}$) mice showed expected increases from 30% mineral by weight in forming enamel to 50% mineral by weight as enamel began to mature to 85–90% mineral by weight in nearly mature enamel (Fig. 4, *B* and *E*). *Klk4*$^{-/-}$ mice showed increases in percent mineral by weight that were almost identical to those occurring in wild-type and heterozygous mice until a level of about 80% mineral by weight in mid-maturation and then remained unchanged thereafter (Fig. 4*B*). *Mmp20*$^{-/-}$ mice showed a trend for having higher percent mineral by weight during the secretory and early maturation stages (Fig. 4*E*, *yellow diamonds*, *locations 1–3 mm* on the mandibular incisor), followed by a slow increase from about 67 to 75% mineral by weight across the maturation stage (Fig. 4*E*, *yellow diamonds*, in *locations 3–9 mm*).

Mineral acquisition rates (mineral gain per mm) within maturing enamel on maxillary and mandibular incisors of wild-type (*Klk4*$^{+/+}$, *Mmp20*$^{+/+}$) and heterozygous (*Klk4*$^{+/-}$, *Mmp20*$^{+/-}$) mice all showed peak levels in mid-maturation around 35–40 μg/mm (Fig. 4, *C* and *F*). Mineral acquisition rates for enamel in *Klk4*$^{-/-}$ mice showed similar trends, but

peak levels were lower by about 15% (Fig. 4*C*). *Mmp20*$^{-/-}$ mice in contrast had mineral acquisition rates in mid-maturation that were roughly 70% below normal, but these mice also showed a continued slow uptake of mineral across the rest of the maturation stage (Fig. 4*F*).

Volatile Content (Mostly Protein) in Developing Enamel from Klk4 and Mmp20 Wild-type, Heterozygous, and Homogzygous Null Mice—Substantial differences were detected between genotypes in the amount of volatiles (mostly protein) vaporized during ashing of enamel samples (Fig. 5*A*). Wild-type mice (*Klk4*$^{+/+}$, *Mmp20*$^{+/+}$) showed the characteristic rodent incisor enamel pattern of increasing amounts of volatiles across the secretory stage to a peak level in early maturation stage followed by a precipitous drop in volatiles as maturation progressed (Fig. 5*A*, *circles*). Heterozygous mice (*Klk4*$^{+/-}$, *Mmp20*$^{+/-}$) showed the same trend for increases and decreases in volatiles as enamel developed except that these samples contained greater amounts of volatiles at the location in maturation when the enamel first became too hard to cut with a scalpel blade (Fig. 5*A*, *squares*, strips 3–4 mm on maxilla and 5–6 mm on mandible). *Klk4*$^{-/-}$ mice showed the same increase in volatiles to a peak amount in early maturation followed by a drop in volatiles, but the decreases in this case were not as great as that occurring in heterozygous or wild-type mice (Fig. 5*A*, *green diamonds*). This was followed by a second increase in volatiles as maturation continued reaching a peak at a site close to where the enamel erupted into the mouth (Fig. 5*A*, *green diamonds*, strips 4–6 mm on maxilla and 6–8 mm on mandible). The amount of volatiles in *Klk4*$^{-/-}$ enamel samples decreased progressively thereafter from the gingival margin to the incisal tip across the erupted portion of the incisor (Fig. 5*A*, *green diamonds,* strips 7–8 mm on maxilla and 9–12 mm on mandible). Incisor enamel of *Mmp20*$^{-/-}$ mice was more than 2-fold thinner than normal (Fig. 3) making direct comparisons of raw data for volatiles between this and other genotypes difficult. In an attempt to circumvent this problem, data on volatiles shown in Fig. 5*A* for *Mmp20*$^{-/-}$ mice were normalized so that all curves in this figure represent enamel having similar thicknesses. In these terms, the enamel in *Mmp20*$^{-/-}$ mice showed the same characteristic rise in volatile content to a peak level in early maturation but only a gradual, as opposed to sharp, decline in volatile content thereafter (Fig. 5*A*, *yellow diamonds*). The amount of volatiles in enamel samples in terms of normalized enamel thickness would be similar to the volatile levels detected in *Klk4*$^{-/-}$ mice by late maturation and along the erupted portions of the incisors where it could be measured (Fig. 5*A*, *yellow versus green diamonds,* strips 5–12 mm).

The end result of these differences in volatiles (Fig. 5*A*) and mineral (Fig. 4, *A* and *D*) content was marked alterations in the mineral-to-volatile ratios between genotypes across the maturation stage (Fig. 5*B*, 2–6 mm on maxilla and 3–8 mm on mandible). For example, at a position in mid-maturation where enamel is normally too hard to cut with a scalpel blade, mineral-to-volatile ratios on mandibular incisors were 9 in wild-type mice (*Klk4*$^{+/+}$, *Mmp20*$^{+/+}$), 6 in heterozygous mice (*Klk4*$^{+/-}$, *Mmp20*$^{+/-}$), 4 in *Klk4*$^{-/-}$ mice, and 2 in *Mmp20*$^{-/-}$ mice (Fig. 5*B*). Interestingly, *Klk4*$^{-/-}$ mice showed a trend for a slight decrease in mineral-to-volatile ratio from mid- to late maturation (Fig. 5*B*, 5–8 mm) and an increasing ratio along the erupted portion of the tooth from gingival margin to incisal tip (Fig. 5*B*, 9–12 mm). *Mmp20*$^{-/-}$ mice on the other hand showed a trend for progressively increasing mineral-to-protein ratio from 2 to 4 from mid- to late maturation stage (Fig. 5*B*,

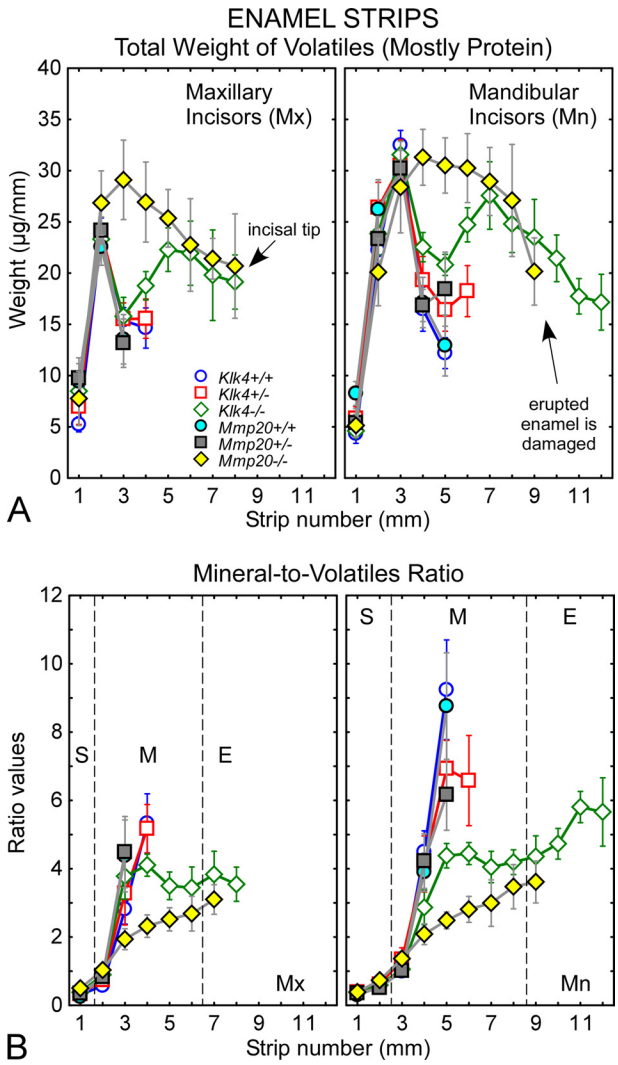

FIGURE 5. **Protein content in enamel.** Total dry weight of volatiles (*A*) and mineral-to-volatiles ratio (*B*) for developing enamel on incisors from wild-type (*Klk4*$^{+/+}$; *Mmp20*$^{+/+}$), heterozygous (*Klk4*$^{+/-}$; *Mmp20*$^{+/-}$), and null (*Klk4*$^{-/-}$; *Mmp20*$^{-/-}$) mice. The *graphs* in *A* and *B* represent mean ± 95% confidence intervals for 1-mm-long enamel strips microdissected from maxillary (*left graph* each panel, *Mx*) and mandibular (*right graph* each panel, *Mn*) incisors. Stages of amelogenesis are illustrated by the *dashed lines* in *B* (*S*, secretory stage; *M*, maturation stage; *E*, erupted portion). Weight data for *Mmp20*$^{-/-}$ mice in *A* were normalized so that genotypes are compared relative to enamel having the same overall thickness. The enamel in both *Klk4*$^{-/-}$ and *Mmp20*$^{-/-}$ mice contains excess amounts of volatiles (mostly protein) throughout the maturation stage (*A*). *Klk4*$^{-/-}$ mice show an initial loss of volatiles in early to mid-maturation as occurs in normal enamel development, but the decline is less and is followed by a rise in volatiles during late maturation and decline across the erupted portion of the tooth (*A, green diamonds*). *Mmp20*$^{-/-}$ mice maintain relatively high amounts of volatiles throughout the maturation stage (*A, yellow diamonds*). A mild heterozygous effect in volatile content is evident at mid-maturation on mandibular incisors of both *Klk4*$^{+/-}$ and *Mmp20*$^{+/-}$ mice (*A, strip 5, squares*). Mineral-to-volatiles ratios are consistently low throughout maturation in *Klk4*$^{-/-}$ mice and show a trend to rise across the erupted portion of the incisor (*B*). Mineral-to-volatiles ratios are even lower in *Mmp20*$^{-/-}$ mice but show a trend to rise across the maturation stage and onto the erupted portion of the tooth (*B*).

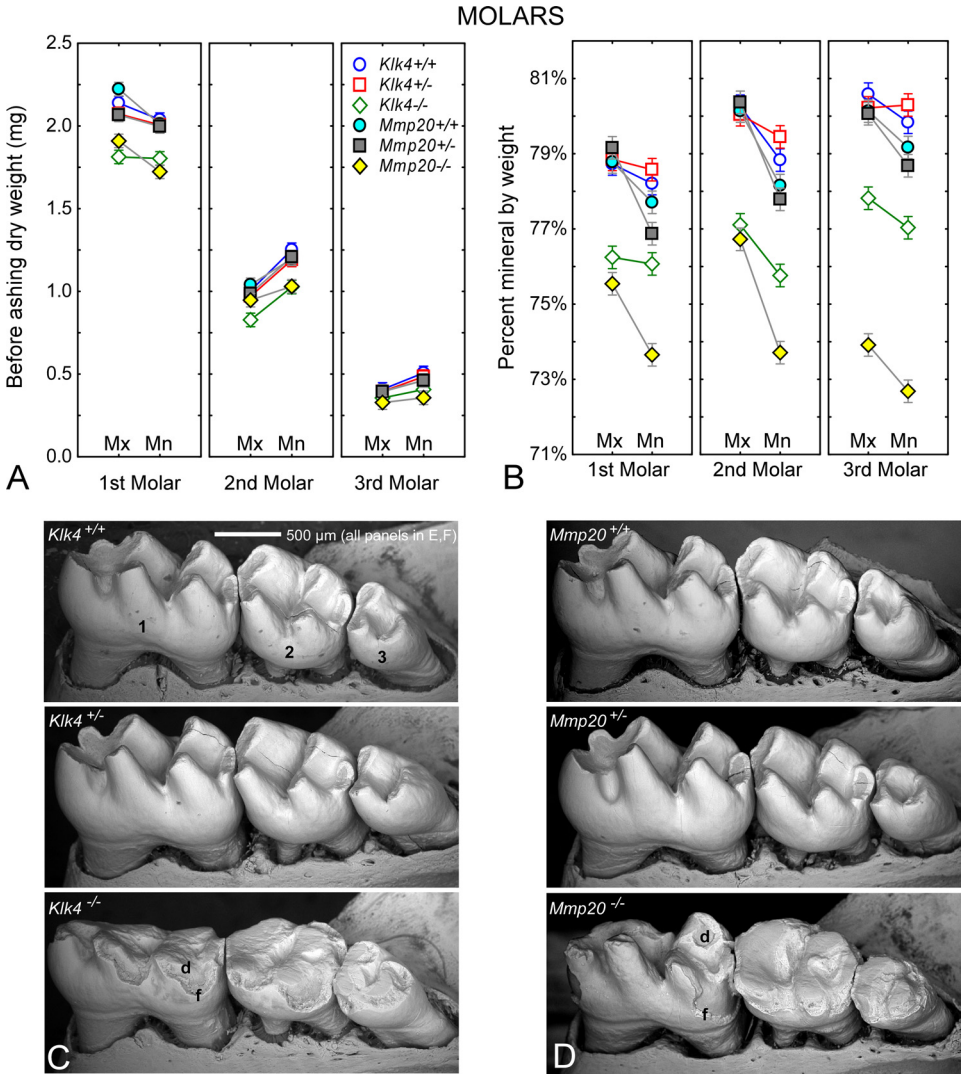

FIGURE 6. **Mineral content in molars.** *A,* mean plots ± 95% confidence intervals of the before ashing dry weights (*A*) of the 1st, 2nd, and 3rd maxillary (*Mx*) and mandibular (*Mn*) molars in wild-type (*Klk4*$^{+/+}$; *Mmp20*$^{+/+}$), heterozygous (*Klk4*$^{+/-}$; *Mmp20*$^{+/-}$), and null (*Klk4*$^{-/-}$; *Mmp20*$^{-/-}$) mice. Alterations in enamel mineralization and excessive coronal wear due to loss-of-function of Klk4 and Mmp20 are detectable as reduced gross weight of the molars. *B,* mean plots ± 95% confidence intervals of the percent mineral by weight for molars in the six genotypes. A molar without enamel would have a percent mineral content of 71–73% by weight (see Table 1). Third and to a lesser extent second molars show the greatest relative changes in mineral content. *C* and *D,* scanning electron microscopy in backscatter mode of the 1st, 2nd, and 3rd mandibular molar crowns from wild-type (*C, Klk4*$^{+/+}$; *D, Mmp20*$^{+/+}$), heterozygous (*C, Klk4*$^{+/-}$; *D, Mmp20*$^{+/-}$), and null (*C, Klk4*$^{-/-}$; *D, Mmp20*$^{-/-}$) mice. Cracks within some molar crowns are artifacts from freeze drying. The enamel covering the crowns of molars contributes to the overall weight of these teeth and is subject to change as the molar crowns wear down by occlusal attrition. Developmentally weakened and hypomineralized enamel in homozygous mice fractures (*f*) off the crowns and abrades more easily thereby exposing areas of dentin (*d*) to severe attrition.

5–8 mm). The same trends were apparent on maxillary incisors (Fig. 5*B*, 3–8 mm).

Mineral Content in Dentin and in Maxillary and Mandibular Bone and Intact Whole Molars from Klk4 and Mmp20 Wild-type, Heterozygous and Homogzygous Null Mice—No differences in mineral content by genotype were detected for either dentin or bone (Table 1). As noted in a previous study (21), intact whole molars had differences in gross dry weights and mineral content related to molar type (1st, 2nd, and 3rd) jaw (*Mx* and *Mn*) and genotype (*Klk4*, *Mmp20*) (Fig. 6*A*). There was a mild homozygous effect for lower starting dry weights of molars from *Klk4*$^{-/-}$ and *Mmp20*$^{-/-}$ mice (Fig. 6*A*) due in part to severe occlusal wear evident on the null teeth (Fig. 6, *C* and *D*). The percent mineral by weight was 77–80% in all molars from wild-type (+/+) and heterozygous (+/−) mice, about 76–77% in molars from *Klk4*$^{-/-}$ mice, and around 72–76% in molars from *Mmp20*$^{-/-}$ mice (Fig. 6*B*).

DISCUSSION

The results of this study provide some very interesting insights into the roles that Klk4 and Mmp20 play in the well established inverse relationship between protein loss and mineral gain during enamel development (1, 12). However, before attempting to interpret these findings, it is important to note that expression of the genes for these two proteinases appears completely independent of each other (6). Hence, *Klk4* null mice express Mmp20, and *Mmp20* null mice express Klk4 (26). This is clearly supported in this study by findings that *Klk4* null mice produce enamel that is normal in thickness and basic substructure (Fig. 3), which they would not do if Mmp20 function

was severely depressed or missing. *Mmp20* null mice show a trend for relative increases in enamel mineralization across the maturation stage (Fig. 5*B*), which would not happen if Klk4 was missing and/or if Mmp20 was the only proteinase capable of activating Klk4 from its proenzyme state (14, 27). However, the mild hypomineralization and structural defects in enamel organization occurring near the DEJ in *Klk4* null mice, which ultimately prove fatal to resistance against compressive forces at incisal edges and cusp tips when these teeth erupt into functional occlusion, resemble a mild form of the more severe abnormalities present at this location in *Mmp20* null mice (Fig. 3). This suggests that initial expression of Mmp20 at the start of amelogenesis could be somewhat depressed in *Klk4* null mice. Alternatively, there may be a window in time at the start of enamel development when Klk4 is briefly expressed and activated as ameloblasts start forming enamel rods. Some evidence has been presented suggesting that odontoblasts express Klk4 at this time and could serve this function (28, 29). However, initial studies with the Klk4 knock-out/*lacZ* knock-in mouse model did not reveal any LacZ-staining nuclei in young or old odontoblasts leaving this question unresolved at this time (9).

It is further assumed that substrate specificities and levels of hydrolytic activity of Klk4 and Mmp20 remain relatively normal in each opposing loss-of-function mouse model. Hence, the Mmp20 present in developing enamel of *Klk4* null mice presumably is produced and secreted throughout the secretory stage of amelogenesis and creates the same multiple series of fragments from hydrolysis of amelogenin and ameloblastin at the same cleavage sites as those occurring normally (16, 17). The matrix proteins retained in maturing enamel of *Klk4* null mice especially in the deepest most regions (Figs. 3 and 5) therefore likely represent a proportional mixture of these fragments or certain specific fragments requiring Klk4 for complete removal (9). The processing of intact enamelin by Mmp20 is presently not well defined (18), but it is known that this proteinase can slowly cleave the 32-kDa enamelin fragment if it is deglycosylated (15). Some of the excess matrix protein in enamel of *Klk4* null mice therefore also likely includes undigested or more slowly digested fragments derived from enamelin (9).

The Klk4 present in developing enamel of *Mmp20* null mice presumably is produced and secreted during transition and within the maturation stage of amelogenesis as occurs in normal mice (11, 26). However, the characteristic initial postsecretory processing and fragmentation that arises from Mmp20 action on amelogenin and ameloblastin (and enamelin) during the appositional growth (secretory) stage does not occur in these animals (7). Hence, Klk4 in *Mmp20* null mice likely acts on more intact and higher molecular weight forms of enamel matrix proteins. Klk4 efficiently hydrolyzes intact recombinant amelogenin and ameloblastin (and enamelin) but at cleavage sites that are distinctly different from Mmp20 thereby creating fragments of various molecular weights not normally seen *in vivo* (16, 17). This suggests that some/most of the excess matrix protein detected in maturing enamel of *Mmp20* null mice, especially in the deepest most regions near the DEJ (Figs. 3 and 5), represents atypical fragments of amelogenin and ameloblastin generated by Klk4 that may be less efficiently removed by modulating ameloblasts (12). These atypical fragments arising from cleavage of more intact forms of amelogenin, ameloblastin, and enamelin by Klk4 in *Mmp20* null mice may be one of the underlying causes leading to abnormalities in enamel structure (Fig. 3) and enamel organ cell organization (7), the latter of which seem to become more severe over time as maturation proceeds to completion (Fig. 1) (7).

One of the most surprising aspects of this study was the degree of hardness to which the outer surface layer of maturing enamel reached on incisors of *Klk4* null mice, comparable with normal incisors in terms of damaging scalpel blades used to make releasing cuts. It was only by repeated scoring with many scalpel blades that any indentations into the tough superficial enamel were possible. Once the surface layer had been breached, the deeper (inner) enamel was physically softer than normal, and 1-mm-long strips of enamel could then be removed manually aided in part by a fracture plane originating from the hypomineralization defect near the DEJ. This is validated in Fig. 3 by the backscattered (SEM) imaging that revealed regional variations in mineral density across the thickness of the enamel layer similar in trend to differences reported for human enamel (high mineral densities at the enamel surface and lower densities near the DEJ) (30, 31). Mineral content in the outermost part of the nearly mature enamel layer in *Klk4* null mice is only about 8% below normal, whereas the middle and innermost regions are about 15 and 20% below normal, respectively (Fig. 3). Interestingly, the enamel on incisors of *Mmp20* null mice, although thin and structurally highly defective, shows practically the same mineralization pattern as *Klk4* null mice in the outermost and middle regions, which contain about 8 and 15% less total mineral per unit area as normal enamel (excluding nodules in the outermost part). The innermost enamel near the DEJ is much more defective and has about 30% less mineral than normal likely representing one of the reasons for why enamel on these teeth fractures away so easily from the dentin (Fig. 3) (32). Hence, even though *Mmp20* null mice express Klk4, this proteinase alone cannot compensate for developmental defects built into the system during the formative (appositional growth) phase of enamel development. Taken together, these *Mmp20* null results are consistent with the idea that resorptive activity by ameloblasts at the surface of enamel contributes in part to the maturation of enamel (12), although such cellular activity by itself cannot drive enamel to its full maturity as revealed by the below normal mineral content present in the erupted enamel covering incisors and molars of *Klk4* null mice (Figs. 5 and 6).

Although analyses of raw mineral content and mineral acquisition rates by themselves suggest only minor effects on enamel development in the incisors of *Klk4* null mice (Fig. 4), much more revealing insights into enamel developmental imbalances in *Klk4* null mice were obtained from strip-by-strip plots of the volatile component in forming and maturing enamel (Fig. 5*A*). As noted in a previous study (20), volatiles are the component of freeze-dried enamel samples that are vaporized during heating at 575 °C. Most of this evaporated material is organic in nature, although some mineral-based carbonate and residual bound water may be released as CO_2 gas and steam (less than 3% of total) (20). Immature acidic forms of hydroxyapatite are also

susceptible to some minor loss of components by heat (as water vapor) (33), but this is a potential problem associated more with the secretory stage that contains forming crystallites than to the maturation stage where existing crystallites merely expand in volume (12). In reference to the organic component itself, the quantity of matrix proteins present in developing enamel at any moment in time is the net difference between the amount of newly formed proteins being added into the enamel layer by secretory activity of ameloblasts *versus* the amount of matrix-resident proteins being lost through proteolytic degradation and outward diffusion and/or resorptive uptake of residual protein fragments into the lysosomal system of ameloblasts (12). It is well established in rodent incisors that the most intense phase of protein release occurs during the secretory stage (strips 0–1.5 maxillary and 0–2.5 mandibular incisor in Fig. 5*A*) (34). The intensity of protein secretion drops precipitously during postsecretory transition and then continues at very low levels up to about mid-maturation (strips 2–3 and 3–5, Fig. 5*A*) (34).

It is evident from Fig. 5*A* that the volatile content of enamel in *Klk4* null mice appears perfectly normal up to early maturation. The initial sharp drop in volatile content characteristic of the change from early to mid-maturation in normal mice also occurs in *Klk4* null mice, but the decline in volatiles is only about 30% as opposed to the 60% decrease seen in normal mice and intermediate decline observed in *Klk4* heterozygous mice (Fig. 5*A*). Therefore, 50% of the loss in volatiles during the first half of the maturation stage is Klk4-dependent and 50% is not, originating from other mechanisms that likely include resorptive activity by ameloblasts (12).

An unanticipated finding was evidence for the addition of new volatiles from mid- to late maturation creating a peak almost as high as the one found in early maturation (strips 4–6 maxillary and 6–8 manibular incisor, respectively, in Fig. 5*A*). This is a region of almost mature enamel that heretofore has been impossible to quantify in normal mice because the enamel is too hard to dissect with scalpel blades and dental tools. However, we have analyzed one other loss-of-function mouse model unrelated to Klk4 where enamel strips could be removed from this same region of the incisor because of disrupted enamel maturation, and we detected no similar increase in volatiles (mandibular incisors of $Enam^{+/-}$ mice) (21). This suggests that the origin for the appearance of the second peak of volatiles in *Klk4* null mice relates entirely to the absence of this proteinase. The cause for the second rise in volatiles is unclear, but one possibility is secretion of protein associated with the yellow ferritin-based pigment that occurs within this region as part of normal rodent incisor enamel development (12, 35–38). An additional role for Klk4 therefore may be to degrade pigment-associated protein so that final pre-eruptive maturation and interlocking of enamel crystallites can be achieved in rodent incisors.

The relatively high content of volatiles present in maturing enamel of *Mmp20* null mice is of interest because these animals express Klk4 (26) yet seem unable to accomplish any net protein loss until the enamel erupts out into the oral cavity (Fig. 5*A*). There have been reports that ameloblast structure and function and normally rigid progression through precisely defined steps of their life cycle are out of balance in *Mmp20* null mice, and maturation stage ameloblasts show pathologies in the form of nodules (7, 39). It is therefore possible that both the timing of transition from the secretory stage to the maturation stage and normal resorptive activity by ameloblasts are altered in these animals. Problems in transition between stages of development is supported by the SEM surface imaging, which indicated a quick secretory to maturation stage change in the center region of the labial surface but more gradual and extended changes toward the mesial and lateral sides of the incisor (as indicated by the lumpy nature of maturation stage enamel in these teeth; Fig. 2*B*, $Mmp20^{-/-}$). One reason for the apparent high levels of enamel volatiles at locations on the tooth that should represent the maturation stage (Fig. 5*A*) may in part arise from an overlap of secretory stage with maturation stage within the three-dimensional context of 1-mm-long strips of enamel (in a sense a "false-positive" for the amount of protein indicated). It is also likely, as suggested by the SEM surface images, that a certain amount of protein originating from cell debris trapped in surface nodules contaminates the enamel samples analyzed by ashing (Fig. 2, *B* and *D*). We also suspect that a certain amount of secretory activity would be required by maturation stage ameloblasts to form the surface nodules that become more prominent relative to the maturation stage in an incisal direction along the length of the incisor (Fig. 2*B*). Hence, it is likely that Klk4 is functioning reasonably normally in *Mmp20* null mice despite the impression of protein overload across the maturation stage.

The mineral-to-volatile curves in Fig. 5*B* provide the best summary regarding what is wrong with enamel development on incisors of *Klk4* and *Mmp20* null and heterozygous mice. As noted by many investigators, there appears to be a critical quantity of organic material that has to be removed from the enamel layer to achieve rapid volumetric expansion of hydroxyapatite crystallites seeded and lengthened during the secretory stage (1, 2). In the case of normal mice, this crystal growth surge occurs over a distance of about 2 mm of tooth length. It elevates the mineral content of enamel by 9-fold (90% mineral by weight on mandibular incisors) relative to its starting level of about 1 part mineral to 1 part volatiles (50% mineral by weight) at the start of the maturation stage (Fig. 5*B*). Over the next 3 mm of tooth length, the mineral content increases only by an additional 5%, but this seems to be critical for bringing the crystallites into their final interlocking state (12). *Klk4* null mice are able to drive mineral growth 4-fold up to mid-maturation (80% mineral by weight), but they are unable to achieve further net increases in mineral content thereafter due in part to a wave of new volatile material (likely protein related to pigmentation) added into the enamel layer between mid- and late maturation (Fig. 5*B*). A small posteruptive, relative increase in mineral content appears to occur in these teeth as the enamel comes into occlusion (Fig. 5*B*). Mineral content is not distributed uniformly across the thickness of the enamel layer in *Klk4* null mice but is highest near the enamel surface and lowest near the DEJ (Fig. 3). There is also a developmental defect in enamel rods where they begin near the DEJ, which makes these teeth less resistant to compressive forces when the teeth occlude one another (Figs. 3 and 6*C*). *Mmp20* null mice produce thin and poorly organized enamel that is only able to increase in mineral

content about 2-fold by mid-maturation (67% mineral by weight; Figs. 4 and 5*B*). This enamel, however, does achieve a further 5% increase in mineral content (to 75% mineral by weight) by late maturation (Fig. 5*B*). There is marked hypomineralization and severe structural defects near the DEJ, which makes *Mmp20* null mouse enamel susceptible to separation from the dentin under light compressive forces (Figs. 3 and 6*D*). Both *Klk4* and *Mmp20* heterozygous mice show slightly delayed maturation of their enamel with initial 6–7-fold increases in mineral content from early to mid-maturation (~87% mineral by weight) and normal levels of mineralization thereafter (to 95% mineral by weight) when fully mature (Fig. 5*B*).

Acknowledgments—We thank Line Mongeon from the Facility for Electron Microscopy Research, McGill University, for assistance with incisor and molar SEM surface imaging (Figs. 2 and 6). We also thank James Hinchcliff from the Department of Geological Sciences, University of Michigan, for expertise in diamond polishing and Carl Henderson from the Electron Microbeam Analysis Laboratory, University of Michigan, for assistance with the SEM imaging of enamel in cross-section (Fig. 3).

REFERENCES

1. Simmer, J. P., Papagerakis, P., Smith, C. E., Fisher, D. C., Rountrey, A. N., Zheng, L., and Hu, J. C. (2010) *J. Dent. Res.* **89,** 1024–1038
2. Lacruz, R. S., Nanci, A., Kurtz, I., Wright, J. T., and Paine, M. L. (2010) *Calcif. Tissue Int.* **86,** 91–103
3. Hu, J. C., Chun, Y. H., Al Hazzazzi, T., and Simmer, J. P. (2007) *Cells Tissues Organs* **186,** 78–85
4. Bei, M. (2009) *Curr. Opin. Genet. Dev.* **19,** 504–510
5. Wright, J. T., Hart, T. C., Hart, P. S., Simmons, D., Suggs, C., Daley, B., Simmer, J., Hu, J., Bartlett, J. D., Li, Y., Yuan, Z. A., Seow, W. K., and Gibson, C. W. (2009) *Cells Tissues Organs* **189,** 224–229
6. Lu, Y., Papagerakis, P., Yamakoshi, Y., Hu, J. C., Bartlett, J. D., and Simmer, J. P. (2008) *Biol. Chem.* **389,** 695–700
7. Caterina, J. J., Skobe, Z., Shi, J., Ding, Y., Simmer, J. P., Birkedal-Hansen, H., and Bartlett, J. D. (2002) *J. Biol. Chem.* **277,** 49598–49604
8. Kim, J. W., Simmer, J. P., Hart, T. C., Hart, P. S., Ramaswami, M. D., Bartlett, J. D., and Hu, J. C. (2005) *J. Med. Genet.* **42,** 271–275
9. Simmer, J. P., Hu, Y., Lertlam, R., Yamakoshi, Y., and Hu, J. C. (2009) *J. Biol. Chem.* **284,** 19110–19121
10. Hart, P. S., Hart, T. C., Michalec, M. D., Ryu, O. H., Simmons, D., Hong, S., and Wright, J. T. (2004) *J. Med. Genet.* **41,** 545–549
11. Hu, J. C., Sun, X., Zhang, C., Liu, S., Bartlett, J. D., and Simmer, J. P. (2002) *Eur. J. Oral. Sci.* **110,** 307–315
12. Smith, C. E. (1998) *Crit. Rev. Oral Biol. Med.* **9,** 128–161
13. Simmer, J. P., Sun, X., Yamada, Y., Zhang, C. H., Bartlett, J. D., and Hu, J. C. (2004) in *Proceedings of the 8th International Symposium on Biomineralization, Niigata, Japan, September 25–28, 2001* (Kobayashi, I., and Ozawa, H., eds) pp. 348–352, Tokai University Press, Hadano, Japan
14. Ryu, O., Hu, J. C., Yamakoshi, Y., Villemain, J. L., Cao, X., Zhang, C., Bartlett, J. D., and Simmer, J. P. (2002) *Eur. J. Oral. Sci.* **110,** 358–365
15. Yamakoshi, Y., Hu, J. C., Fukae, M., Iwata, T., and Simmer, J. P. (2006) *Eur. J. Oral. Sci.* **114,** 45–51
16. Nagano, T., Kakegawa, A., Yamakoshi, Y., Tsuchiya, S., Hu, J. C., Gomi, K., Arai, T., Bartlett, J. D., and Simmer, J. P. (2009) *J. Dent. Res.* **88,** 823–828
17. Chun, Y. H., Yamakoshi, Y., Yamakoshi, F., Fukae, M., Hu, J. C., Bartlett, J. D., and Simmer, J. P. (2010) *J. Dent. Res.* **89,** 785–790
18. Hu, J. C., and Yamakoshi, Y. (2003) *Crit. Rev. Oral Biol. Med.* **14,** 387–398
19. Bartlett, J. D., Beniash, E., Lee, D. H., and Smith, C. E. (2004) *J. Dent. Res.* **83,** 909–913
20. Smith, C. E., Chong, D. L., Bartlett, J. D., and Margolis, H. C. (2005) *J. Bone Miner. Res.* **20,** 240–249
21. Smith, C. E., Wazen, R., Hu, Y., Zalzal, S. F., Nanci, A., Simmer, J. P., and Hu, J. C. (2009) *Eur. J. Oral. Sci.* **117,** 485–497
22. McKee, M. D., Wedlich, L., Pompura, J. R., Nanci, A., Smith, C. E., and Warshawsky, H. (1988) *Arch. Oral Biol.* **33,** 413–423
23. Weber, D. F. (1968) *J. Morphol.* **126,** 435–445
24. Nylen, M. U., Omnell, K. A., and Löfgren, C. G. (1970) *Tandlaegebladet* **74,** 685–695
25. Warshawsky, H. (1971) *Anat. Rec.* **169,** 559–583
26. Tye, C. E., Sharma, R., Smith, C. E., and Bartlett, J. D., (2010) *J. Dent. Res.* **89,** 1421–1426
27. Tye, C. E., Pham, C. T., Simmer, J. P., and Bartlett, J. D. (2009) *J. Dent. Res.* **88,** 323–327
28. Fukae, M., Tanabe, T., Nagano, T., Ando, H., Yamakoshi, Y., Yamada, M., Simmer, J. P., and Oida, S. (2002) *J. Dent. Res.* **81,** 668–672
29. Nagano, T., Oida, S., Ando, H., Gomi, K., Arai, T., and Fukae, M. (2003) *J. Dent. Res.* **82,** 982–986
30. Meredith, N., Sherriff, M., Setchell, D. J., and Swanson, S. A. (1996) *Arch. Oral Biol.* **41,** 539–545
31. He, B., Huang, S., Jing, J., and Hao, Y. (2010) *Arch. Oral Biol.* **55,** 134–141
32. Beniash, E., Skobe, Z., and Bartlett, J. D. (2006) *Eur. J. Oral. Sci.* **114,** 24–29
33. Elliott, J. C. (1994) *Structure and Chemistry of the Apatites and Other Calcium Orthophosphates*, pp. 259–263, Elsevier Science Publishing Co., Inc., New York
34. Smith, C. E., and Nanci, A. (1996) *Anat. Rec.* **245,** 186–207
35. Karim, A., and Warshawsky, H. (1984) *Am. J. Anat.* **169,** 327–335
36. McKee, M. D., Zerounian, C., Martineau-Doizé, B., and Warshawsky, H. (1987) *Anat. Rec.* **218,** 123–127
37. Miyazaki, Y., Sakai, H., Shibata, Y., Shibata, M., Mataki, S., and Kato, Y. (1998) *Arch. Oral Biol.* **43,** 367–378
38. Yanagawa, T., Itoh, K., Uwayama, J., Shibata, Y., Yamaguchi, A., Sano, T., Ishii, T., Yoshida, H., and Yamamoto, M. (2004) *Genes Cells* **9,** 641–651
39. Bartlett, J. D., Skobe, Z., Lee, D. H., Wright, J. T., Li, Y., Kulkarni, A. B., and Gibson, C. W. (2006) *Eur. J. Oral Sci.* **114,** 18–23